



University of
Massachusetts
Amherst

Multidimensional Discrete Compactons in Nonlinear Schrödinger Lattices with Strong Nonlinearity Management

Item Type	article
Authors	D'Ambroise, J.; Salerno, M.; Kevrekidis, P. G.; Abdullaev, F. Kh.
Download date	2026-06-08 09:03:06
Link to Item	https://hdl.handle.net/20.500.14394/34298

Multidimensional discrete compactons in nonlinear Schrödinger lattices with strong nonlinearity management

J. D' Ambroise,¹ M. Salerno,² P. G. Kevrekidis,^{3,4} and F. Kh. Abdullaev^{5,6}

¹*Department of Mathematics and Statistics, Amherst College, Amherst, Massachusetts 01002, USA*

²*Dipartimento di Fisica "E.R. Caianiello," CNISM, and INFN, Gruppo Collegato di Salerno, Università di Salerno, Via Giovanni Paolo II, 84084 Fisciano, Salerno, Italy*

³*Department of Mathematics and Statistics, University of Massachusetts Amherst, Amherst, Massachusetts 01003, USA*

⁴*Center for Nonlinear Studies and Theoretical Division, Los Alamos National Laboratory, Los Alamos, New Mexico 87544, USA*

⁵*Department of Physics, Faculty of Sciences, International Islamic University Malaysia, Jln. Indera Mahkota, Sultan Ahmad Shah, 25200, Kuantan, Malaysia*

⁶*CCNH, Universidade Federal do ABC, 09210-170 Santo André, São Paulo, Brazil*

(Received 12 August 2015; published 19 November 2015)

The existence of multidimensional lattice compactons in the discrete nonlinear Schrödinger equation in the presence of fast periodic time modulations of the nonlinearity is demonstrated. By averaging over the period of the fast modulations, an effective averaged dynamical equation arises with coupling constants involving Bessel functions of the first and zeroth kinds. We show that these terms allow one to solve, at this averaged level, for exact discrete compacton solution configurations in the corresponding stationary equation. We focus on seven types of compacton solutions. Single-site and vortex solutions are found to be always stable in the parametric regimes we examined. Other solutions such as double-site in- and out-of-phase, four-site symmetric and antisymmetric, and a five-site compacton solution are found to have regions of stability and instability in two-dimensional parametric planes, involving variations of the strength of the coupling and of the nonlinearity. We also explore the time evolution of the solutions and compare the dynamics according to the averaged equations with those of the original dynamical system. The possible observation of compactons in Bose-Einstein condensates loaded in a deep two-dimensional optical lattice with interactions modulated periodically in time is also discussed.

DOI: [10.1103/PhysRevA.92.053621](https://doi.org/10.1103/PhysRevA.92.053621)

PACS number(s): 03.75.Lm, 42.65.-k, 42.81.Dp

I. INTRODUCTION

Periodic management of parameters of nonlinear lattices (and continua) is a very attractive technique for the generation of new types of systems or excitations with interesting localization properties [1]. For example, dynamic suppression of (atom and light, respectively) interwell tunneling has been reported experimentally in Bose-Einstein condensates [2] and in optical waveguide arrays [3]. On the other hand, very fast periodic time variation of the nonlinearity, also called the strong nonlinearity management (SNLM) technique, has been recently shown to be quite effective towards inducing compactly supported (so-called compacton) solutions in lower-dimensional discrete systems such as a one-dimensional (1D) one and two-component Bose-Einstein condensates (BECs) in optical lattices or arrays of nonlinear optical waveguides described by the discrete nonlinear Schrödinger (DNLS) equation [4,5]. The main feature of such solutions, unlike other types of nonlinear excitations such as discrete breathers and intrinsic localized modes, is that their amplitudes decay to zero sharply without any tails. It has been shown for the 1D case that the lack of exponential tails is a consequence of the nonlinear dispersive interaction induced by the SNLM, which permits the vanishing of the intersite tunneling at compacton edges. The absence of tails implies that compactons cannot interact with each other until they are in contact. In the lattice realm, this potentially allows for the possibility of maximal localization in the form of a single-site solution.

Compactons are quite generic in nonlinear continua [6,7] (in one and also higher [8] dimensions) and lattices [9,10] (including compact breathers [11] and quantum analogs [12])

bearing nonlinear dispersion. The difficulty of implementing this condition in physical contexts has largely restricted the investigations mainly to the mathematical side, although this situation is now rapidly changing. Besides BECs under SNLM, physical compactons were suggested to appear also in exciton-polariton condensates [13] and nearly compact (doubly exponential) traveling waves have also been identified in the realm of granular crystals bearing purely nonlinear interactions [14]. Finally, another area of significant interest has recently arisen where special solutions in the form of discrete compactons may emerge. This is due to the existence of so-called flat bands in the linear dispersion relation (due to the geometric characteristics of the corresponding lattice, such as the kagome lattice) [15]. A realization of this type emerged very recently in the realm of the so-called Lieb photonic lattices [16].

Among the above different (Klein-Gordon, nonlinear Schrödinger, Fermi-Pasta-Ulam, etc.) model equations in which compactly supported structures have been proposed, the relevant variants of DNLS are arguably among the most widely applicable as models both for BECs and for nonlinear optics. In the presence of SNLM, this type of system supports discrete compactons via a site-dependent nonlinear rescaling of the interwell tunneling (see [4] for details). A similar approach, applied to the quantum version of the DNLS model, i.e., to the Bose-Hubbard model with time-dependent on-site interaction, has been shown to be quite effective for creating new quantum phases in BECs with compacton-type excitations [17,18] as well as for the generation of density-dependent synthetic gauge fields [19].

These studies have mainly focused on the one-dimensional case. On the other hand, it is known that compactons can

exist also in multidimensional contexts. In particular, multidimensional compactons have been investigated in continuous models such as (two-dimensional) variants of the Korteweg–de Vries equations with nonlinear dispersion [8], relativistic scalar field theories in two dimensions [20], Klein-Gordon and nonlinear Schrödinger equations with sublinear forces, etc. In these last cases, however, the mechanism leading to compacton formation is not the nonlinear dispersion but the presence of a subquadratic interaction potential that enforces compact patterns with sharp fronts [21,22]. In this context, the existence of vortex compactons was also demonstrated to be possible, although only with a finite lifetime [22].

We note in passing here that the stabilization of two-dimensional matter-wave bright solitons [23] and the suppression of collapse [24] was also demonstrated to be possible by means of rapidly oscillating scattering lengths via Feshbach resonance. Furthermore, multidimensional gap solitons can exist in optical lattices as stable excitations for both repulsive [25] and attractive [26] interactions. The connection of such excitations to the ones proposed below may be an interesting topic for future study.

In the discrete case, multidimensional compactons have been scarcely investigated and only in the special case as an example of compact coherent structures in the presence of a flat band of the linear spectrum [15,16]. General case examples (different numbers of sites, including ones bearing vorticity) of multidimensional discrete compactons of the nonlinear Schrödinger type, amenable to physical applications in BECs and nonlinear optics, have only been reported in a very limited number of studies; in fact, the only one that we are aware of is [27].

The aim of this paper is to demonstrate and systematically explore the existence and stability of multidimensional lattice compactons in the discrete nonlinear Schrödinger equation in the presence of periodic time modulations of the nonlinearity i.e., in a two-dimensional generalization of [4] bearing the potential for a wide range of additional structures. In this work we concentrate mainly on compactons localized on no more than five interacting neighboring sites of a 2D square lattice; of particular interest, in addition to the stable single-site compacton, is the stable four-site compacton vortex solution, i.e., bearing a vortical phase structure. In particular, the existence and stability properties of DNLS compacton excitations are investigated both for generic time-dependent nonlinear modulations and in the SNLM limit for which an effective averaged DNLS model is derived. We show that single-site compactons are stable in the whole parameter space, however, two-site compactons have finite stability ranges (although bearing some nontrivial differences from the standard DNLS model), different for symmetric and antisymmetric types and with different dynamical features. Interestingly, stationary three-site compactons with real amplitude cannot exist in the square geometry, while four-site compactons of the symmetric or antisymmetric types exist but have finite regions of instability similar to the double-site configurations. On four nearest-neighbor sites, however, for all values in the parameter space, one has a stable vortex compacton in which the phase of the wave function increases by $\pi/2$, moving clockwise from one corner to the next of the square. Since compactons interact only when they are in contact, one can obviously construct

arbitrary single- and two-site compacton patterns by placing them on noninteracting sites (for example, next-neighbor sites along a diagonal). We also show that five-site compactons with C_4 symmetry can exist and can be stable; their regions of instability are finite, similar to other configurations' instability.

The paper is organized as follows. In Sec. II we introduce the model equation of a 2D DNLS with SNLM and discuss the theoretical derivation of the effective averaged equations with nonlinear dispersion. In Sec. III we derive the existence conditions for exact compacton solutions of the averaged DNLS equation and in Sec. IV we study numerically the linear stability properties and compare results with direct numerical integrations of the original (unaveraged) DNLS system. In Sec. V we discuss briefly the potential future experimental implementations, and summarize our main results.

II. MODEL AND THEORETICAL SETUP

Consider the 2D DNLS equation [28]

$$i\dot{u}_{n,m} + k(u_{n+1,m} + u_{n-1,m}) + \tilde{k}(u_{n,m+1} + u_{n,m-1}) + (\gamma_0 + \gamma(t))|u_{n,m}|^2 u_{n,m} = 0, \quad (1)$$

which serves as a model for the dynamics of BEC in optical lattices subjected to SNLM (through varying the interatomic scattering length by external time-dependent magnetic fields via a Feshbach resonance) [29] as well as for light propagation in 2D optical waveguide arrays [30]. In the latter case, where this type of modulation has been realized not only in discrete but also in continuum media (in both one and higher dimensions) [31], the evolution variable is the propagation distance. Hence, here the SNLM consists of periodic space variations of the Kerr nonlinearity along the propagation direction with the coupling constants k, \tilde{k} quantifying the tunneling between adjacent sites along the n and m directions, respectively, γ_0 denoting the on-site constant nonlinearity and $\gamma(t)$ representing the time-dependent modulation (of the interatomic interactions or of the refractive index, in atomic and optical settings, respectively). In the following we assume a strong management case with $\gamma(t)$ being a periodic, e.g., $\gamma(t) = \gamma(t + T_0)$, and rapidly varying function. As a prototypical example we use $\gamma(t) = \frac{\gamma_1}{\varepsilon} \cos(\Omega t)$, with $\gamma_1 \sim O(1)$, $\varepsilon \ll 1$, $\tau = t/\varepsilon$ denoting the fast time variable, and $T = 2\pi/\Omega$ the period with respect to τ ($T_0 = \varepsilon T$). In the following we take, for simplicity, the coupling constants k, \tilde{k} to be the same for the two directions (assuming square symmetry): $k = \tilde{k} \equiv \kappa$.

The existence of compacton solutions of Eq. (1) in the SNLM limit can be inferred from (and analyzed in the context of) an effective averaged 2D DNLS equation obtained by averaging out the fast time τ . The following averaging procedure is valid only when the frequency of $\gamma(t)$ is very large in comparison to characteristic frequencies of the system; this condition is ensured by our restriction of parameters $\varepsilon \ll 1$ and $\gamma_1, \Omega \sim O(1)$. To that effect, it is convenient to perform the transformation [32] $u_{n,m}(t) = v_{n,m}(t)e^{i\Gamma|v_{n,m}(t)|^2}$ with $\Gamma = \int_0^t dt \gamma(t) = \gamma_1 \Omega^{-1} \sin(\Omega t)$, which allows one to rewrite Eq. (1) as

$$i\dot{v}_{n,m} = \Gamma v_{n,m}(|v_{n,m}|^2)_t - \kappa X - \gamma_0 |v_{n,m}|^2 v_{n,m}, \quad (2)$$

with

$$X = v_{n+1,m} e^{i\Gamma\theta_+^m} + v_{n-1,m} e^{i\Gamma\theta_-^m} + v_{n,m+1} e^{i\Gamma\theta_+^+} + v_{n,m-1} e^{i\Gamma\theta_-^-}, \quad (3)$$

$$\theta_{\pm}^m = |v_{n\pm 1,m}|^2 - |v_{n,m}|^2, \quad \theta_n^{\pm} = |v_{n,m\pm 1}|^2 - |v_{n,m}|^2.$$

On the other hand, $(|v_{n,m}|^2)_t = (\dot{v}_{n,m} v_{n,m}^* + v_{n,m} \dot{v}_{n,m}^*) = i\kappa(v_{n,m}^* X - v_{n,m} X^*)$, with the asterisk denoting complex conjugation. Substituting this expression into Eq. (2) and averaging the resulting equation over the period T of the rapid modulation, we obtain

$$i\dot{v}_{n,m} = i\kappa|v_{n,m}|^2\langle\Gamma X\rangle - i\kappa v_{n,m}^2\langle\Gamma X^*\rangle - \kappa\langle X\rangle - \gamma_0|v_{n,m}|^2 v_{n,m}, \quad (4)$$

with $\langle\cdot\rangle \equiv \frac{1}{T} \int_0^T (\cdot) d\tau$ denoting the fast time average. The averaged terms in Eq. (4) can be calculated by means of the elementary integrals $\langle e^{i\Gamma\theta_{\pm}} \rangle = J_0(\alpha\theta_{\pm})$ and $\langle \Gamma e^{\pm i\Gamma\theta_{\pm}} \rangle = \pm i\alpha J_1(\alpha\theta_{\pm})$, with J_i being Bessel functions of order $i = 0, 1$ and $\alpha = \gamma_1/\Omega$, thus giving

$$i\dot{v}_{n,m} = F(v) \quad (5)$$

with

$$F(v) = -\gamma_0|v_{n,m}|^2 v_{n,m} - \alpha\kappa v_{n,m} [(v_{n+1,m} v_{n,m}^* + v_{n+1,m}^* v_{n,m}) J_1(\alpha\theta_+^m) + (v_{n,m+1} v_{n,m}^* + v_{n,m+1}^* v_{n,m}) J_1(\alpha\theta_n^+) + (v_{n-1,m} v_{n,m}^* + v_{n-1,m}^* v_{n,m}) J_1(\alpha\theta_n^-) + (v_{n,m-1} v_{n,m}^* + v_{n,m-1}^* v_{n,m}) J_1(\alpha\theta_-^-)] - \kappa [v_{n+1,m} J_0(\alpha\theta_+^m) + v_{n,m+1} J_0(\alpha\theta_n^+) + v_{n-1,m} J_0(\alpha\theta_n^-) + v_{n,m-1} J_0(\alpha\theta_-^-)]. \quad (6)$$

Note that the parameters $\gamma_1, \Omega \sim O(1)$ and the averaged equation is valid for times $t \leq 1/\epsilon$. This modified DNLS equation can be written as $i\dot{v}_{n,m} = \delta H_{av}/\delta v_{n,m}^*$, with the averaged Hamiltonian

$$H_{av} = - \sum_{n,m} \left(\kappa J_0(\alpha\theta_+^m) [v_{n+1,m} v_{n,m}^* + v_{n+1,m}^* v_{n,m}] + \kappa J_0(\alpha\theta_n^+) [v_{n,m+1} v_{n,m}^* + v_{n,m+1}^* v_{n,m}] + \frac{\gamma_0}{2} |v_{n,m}|^4 \right).$$

It is interesting to note that this Hamiltonian, except for the rescaling of the coupling constants $k \rightarrow \kappa J_0(\alpha\theta_+^m)$ and $\tilde{k} \rightarrow \kappa J_0(\alpha\theta_n^+)$, is the same as the Hamiltonian of the DNLS equation in the absence of SNLM (e.g., with $\gamma_1 = 0$). A similar rescaling was reported also for the 1D case [4]. It is also worth noting that while the appearance of the Bessel function is intimately connected with harmonic modulations, the existence of compacton solutions and the lattice tunneling suppression is generic for periodic SNLM.

The generalization of these equations to the case of the 3D DNLS equation with cubic lattice symmetry is also quite straightforward to derive (omitted here for brevity). In our numerical results below, we will restrict our considerations to the numerically more tractable 2D case (also more physically realistic at least in the optics realm where the z direction plays the role of the propagation direction).

III. EXACT 2D COMPACTONS

To demonstrate the existence of *exact* compactons in the averaged system, we seek stationary solutions of the form $v_{n,m} = A_{n,m} e^{-i\mu t}$ with $A_{n,m} \in \mathbb{C}$ for which Eq. (5) becomes

$$\mu A_{n,m} = F(A) \quad (7)$$

for F given by Eq. (6). In the following, we theoretically predict and numerically verify that exact solutions of this equation can exist in the form of genuine compactons, i.e., possessing vanishing tails.

The existence of compactons can be intuitively understood in analogy to the shaking of linear optical lattices, which is known to lead to a uniform rescaling of the tunneling constant [33]. One can expect a similar phenomenon to occur for time-modulated interactions but with nonuniform rescalings that depend on the local density, due to cubic nonlinearity. This dependence makes it possible to suppress tunneling only at the boundaries of the excitation, leading to the compacton formation, as demonstrated below. That is, for a sequence of amplitudes associated with the zeros of the Bessel function, tunneling will be suppressed; if this is achieved throughout the boundaries of the relevant coherent structure, the solution will be genuinely compact.

To search for compacton solutions, we begin by applying (7) at any zero-amplitude site that has exactly one out of its four neighbors nonzero. We label this nonzero site $A_{N,M} \neq 0$ and we call it an edge site of the compacton. For $\kappa \neq 0$, this gives the condition

$$J_0(\alpha|A_{N,M}|^2) = 0 \Rightarrow |A_{N,M}|^2 = z_j/\alpha, \quad (8)$$

where z_j is the j th zero of the Bessel function J_0 . In other words, each edge site of the compacton has amplitude

$$A_0 \stackrel{\text{def}}{=} \sqrt{z_j/\alpha}. \quad (9)$$

Applying (7) at edge site (or sites) of the compacton gives an additional condition (or conditions) that depend on the shape of the compacton. We will focus on the following shapes, although other configurations are possible: a single-site solution, a double-site in-phase solution, a double-site out-of-phase solution, three types of four-site solutions in the form of symmetric, asymmetric, and vortex excitations, and finally a five-site configuration. Figures 1 and 2 show one example of each of these configurations. Here L represents the horizontal (and vertical) length of the lattice.

For a single-site compacton solution located at (n_0, m_0) , this nonzero site is an edge site, so it has amplitude A_0 . Taking $A_{n_0, m_0} = A_0$ and applying (7) at (n_0, m_0) gives the value

$$\mu = -\gamma_0 A_0^2. \quad (10)$$

It is interesting to notice that this solution coincides with the one obtained for the one-dimensional DNLS equation under SNLM in Ref. [4]. This is due to the fact that for a single site the compact nature of the solution does not allow it to distinguish one dimension from two or even three dimensions (this is true for a 3D cubic lattice as well). Similar to the 1D case, the single-site compactons are stable; we will see this in more detail in Sec. IV.

For a double-site compacton located at (n_0, m_0) and $(n_0 + 1, m_0)$ (or any other adjacent pair of indices), each with

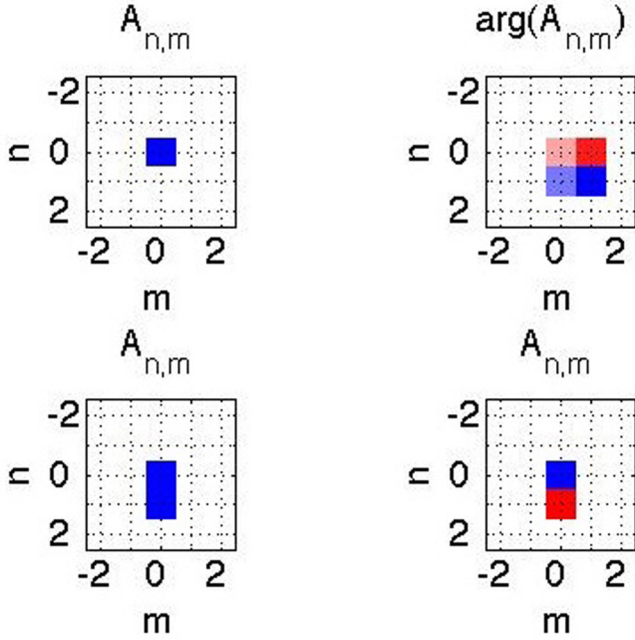


FIG. 1. (Color online) We plot typical examples of exact 2D compacton solutions of Eq. (7). In the top left panel we show a single-site solution, in the bottom left we show a double-site in-phase solution, and in the bottom right we show a double-site out-of-phase solution. In these three plots colors show the (real) values of $A_{n,m}$, where blue represents $A_{n,m} = A_0$ and red $A_{n,m} = -A_0$. No color represents zero amplitude. In the top right plot we show a vortex solution where the four central colored sites all have amplitude A_0 and $\arg(v_{n,m}) \in \{-\pi/2, 0, \pi/2, \pi\}$ is plotted by the four respective colors: dark red, light red, light blue, and dark blue. Here the length and width of the 2D grid are each $L = 7$.

amplitude A_0 , there are the two possibilities: $A_{n_0+1,m_0} = \pm A_{n_0,m_0}$, where plus denotes an in-phase solution and minus an out-of-phase solution. Using that $J_1(0) = 0$ and $J_0(0) = 1$, application of (7) at either of the two nonzero sites then gives

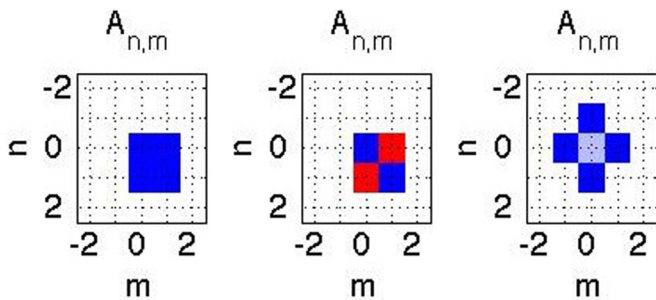


FIG. 2. (Color online) The plots show three additional examples of exact 2D compacton solutions of Eq. (7) on four and five lattice sites. In the left and middle panels symmetric and antisymmetric four-site compactons are shown, respectively, while the right panel depicts a five-site compacton. Dark blue and red colors are as in Fig. 1. The light blue color at the center of the rightmost plot represents the value y for the center site of the five-site solution obtained from Eq. (16).

the value

$$\mu = \mp k - \gamma_0 A_0^2, \tag{11}$$

where the minus corresponds to the in-phase solution and the plus to the out-of-phase solution.

From the above cases one could expect that, although with different stability properties, 1D compactons located on the lattice along n or m directions could be also solutions of multidimensional lattices. This, however, except for the cases considered above, is not true in general. In this respect, one- and two-site compactons are very special, since the number of edge sites in these solutions does not change with dimensionality their analytical expressions, which remain the same in one, two, and three dimensions. For compactons with more than two sites, however, this is not true. Thus, for three-site compactons with real amplitudes $(\dots, 0, A_1, A_2, A_1, 0, \dots)$, in the n direction and zero amplitudes in all other sites, for example, one has three edge sites in two dimensions but only two in one dimension. In contrast with the 1D case, where solutions with real amplitudes exist for arbitrary choices of parameters and are stable [4], the constraints resulting from Eq. (7) can be satisfied only for particular choices of parameters, e.g., real amplitude three-site compactons of the 2D DNLS equation under SNLM are not generic solutions in parameter space.

Genuine 2D compacton solutions first occur on four neighboring sites of a lattice cell. These square compactons can be either symmetric or antisymmetric (see Fig. 2). In either case all four nonzero sites are edge sites with amplitude A_0 . Denoting by (n_0, m_0) the coordinates of the top left corner of the four-site compacton, the symmetric solution has plus signs on the four nonzero sites so that

$$A_{n_0,m_0} = A_{n_0+1,m_0} = A_{n_0,m_0+1} = A_{n_0+1,m_0+1} = A_0.$$

The antisymmetric solution has an alternating pattern of pluses and minuses of the form

$$\begin{aligned} A_{n_0,m_0} &= A_{n_0+1,m_0+1} = A_0, \\ A_{n_0+1,m_0} &= A_{n_0,m_0+1} = -A_0, \end{aligned}$$

with vanishing amplitudes $A_{n,m} = 0$ on all other sites. Substituting the above expressions into Eq. (7), one readily gets the following equation for μ to be satisfied:

$$\pm 2k + A_0^2 \gamma_0 + \mu = 0, \tag{12}$$

with the plus and minus signs referring to the symmetric and antisymmetric cases, respectively.

Quite remarkably, the DNLS system under SNLM can also support discrete vortex compactons. In particular, for a 2×2 shaped vortex solution with the top left nonzero site located at index (n_0, m_0) , all four sites are edge sites with amplitude A_0 . Then we can write

$$\begin{aligned} A_{n_0,m_0} &= A_0, & A_{n_0,m_0+1} &= A_0 e^{-i\pi/2}, \\ A_{n_0+1,m_0} &= A_0 e^{i\pi/2}, & A_{n_0+1,m_0+1} &= A_0 e^{i\pi} \end{aligned} \tag{13}$$

and (7) applied on any of the four vortex sites gives

$$\mu = -\gamma_0 A_0^2. \tag{14}$$

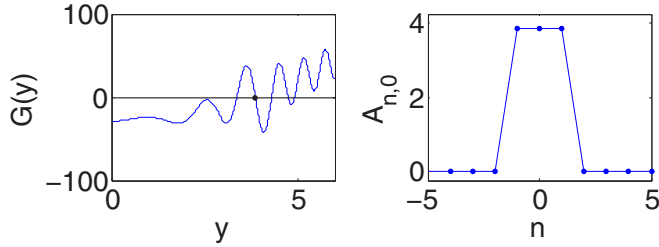


FIG. 3. (Color online) The plots show the graphical solution of Eq. (16) written as $G(y) = 0$ (left panel) and the section at $m = 0$ of a five-site compacton solution (right panel) of Eq. (7) for parameter values $\kappa = 0.5$, $\alpha = 1$, and $\gamma_0 = 2$ with amplitudes at the edge sites fixed in correspondence with the fifth zero z_5 of the Bessel function J_0 , e.g., $A_0 = \sqrt{z_5/\alpha} \approx 3.864$. The amplitude of the central site is taken as the zero of $G(y)$ at $y \approx 3.8695$ (black dot in the left panel), while the corresponding chemical potential is obtained from Eq. (15) as $\mu \approx -30.678$.

With some additional effort it is possible to obtain exact compacton solutions involving more than four nonzero sites. As an example, consider the case of a five-site compacton shaped as in the right panel of Fig. 2. Let (n_0, m_0) denote the index of the center site of the configuration and define $y \equiv A_{n_0, m_0}$. The four edge sites of the five-site solution have amplitudes A_0 , so we take $A_{n_0+1, m_0} = A_{n_0-1, m_0} = A_{n_0, m_0+1} = A_{n_0, m_0-1} = A_0$. Notice that the four edge sites (dark blue in the right panel of Fig. 2) isolate the central (light blue) site from the bulk, reproducing the same situation occurring for a three-site compacton in one dimension (in three dimensions a similar solution would imply a seven-site compacton). Plugging the above edge site expressions into Eq. (7), applied at any one of the four edge sites, then gives an expression fixing the chemical potential

$$\mu(y) = -\kappa \frac{y}{A_0} J_0(\xi(y)) - \gamma_0 A_0^2 + 2\alpha\kappa A_0 y J_1(\xi(y)), \quad (15)$$

where $\xi(y) = \alpha(A_0^2 - y^2)$. The final constraint is obtained by applying Eq. (7) at the center site (n_0, m_0) . Combining the result with the expression in Eq. (15) for μ shows that the amplitude y at the center site must be a solution of the equation $G(y) = 0$ for

$$G(y) \equiv \kappa \left(\frac{4A_0}{y} - \frac{y}{A_0} \right) J_0(\xi(y)) - \frac{\gamma_0}{\alpha} \xi(y) + 10\alpha\kappa A_0 y J_1(\xi(y)). \quad (16)$$

Although Eq. (16) does not yield a simple analytical expression for y , it can be easily solved numerically providing an exact five-site compacton with chemical potential given by Eq. (15). In general, for fixed parameters and a fixed value for $A_0 = \sqrt{z_n/\alpha}$, more than one zero can exist for G (see the left panel of Fig. 3), although not all of them necessarily lead to stable compactons. It is remarkable, however, that some of them can have nonvanishing intervals or ranges of stability in parameter space. We now turn to the details of the stability considerations.

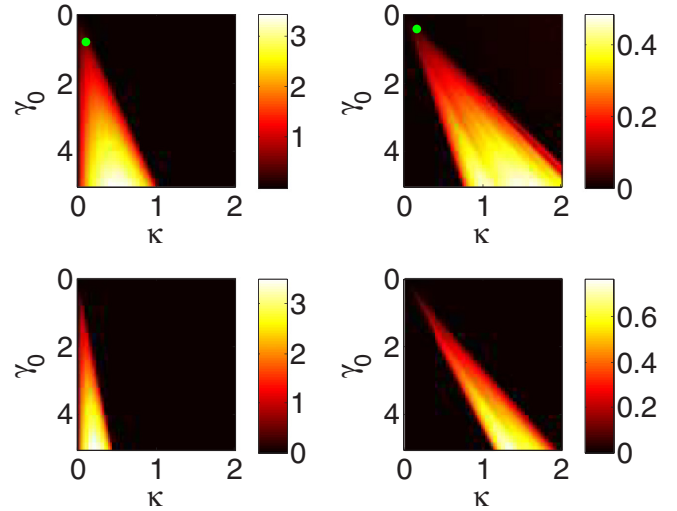


FIG. 4. (Color online) We plot $\max[\text{real}(v)]$ in order to show the strength of the instabilities and regions of stability. Parameter values common across all four plots are $\epsilon = 0.01$ and $\Omega = \gamma_1 = 10$ so that $\alpha = 1$. The left column of plots is associated with a double-site in-phase solution with lattice length both horizontally and vertically $L = 17$. The right column of plots is associated with a double-site out-of-phase solution with lattice length $L = 15$. The top row corresponds to $j = 1$ and the bottom to $j = 2$. Notice that the top right plot shows more striations in the coloring than the top left plot; these further smooth out with higher lattice size L . The green dots in the top two plots are parameter values for which the unstable solutions are propagated in time (see Figs. 7 and 8 below).

IV. STABILITY ANALYSIS AND NUMERICAL SIMULATIONS

In order to examine the stability of the solutions found in Sec. III we set

$$v_{n,m}(t) = (A_{n,m} + \delta e^{vt} \psi_{n,m}) e^{-i\mu t}, \quad (17)$$

where both $A_{n,m}$ and $\psi_{n,m}$ are independent of time t . One can then show that for $\psi_{n,m} = a_{n,m} + ib_{n,m}$ the real vector $\begin{pmatrix} a_{n,m} \\ b_{n,m} \end{pmatrix}$ (with $2L^2$ components) is an eigenvector of the $2L^2 \times 2L^2$ matrix

$$M = \begin{bmatrix} -\frac{\partial \text{Im}[F(\psi)]}{\partial a} & -\frac{\partial \text{Im}[F(\psi)]}{\partial b} \\ \frac{\partial \text{Re}[F(\psi)]}{\partial a} & \frac{\partial \text{Re}[F(\psi)]}{\partial b} \end{bmatrix} \quad (18)$$

with eigenvalue v .

We find that the single-site and vortex solutions are stable for all parameter values κ, λ_0 so that $\max[\text{real}(v)] = 0$; in other words, the nonzero sites' time-evolution plots according to the averaged equation (5) even under perturbation does not lead to growth. The time evolution of the single-site or vortex solution according to the original equation (1) with the time-periodic nonlinearity gives the expected result of oscillations about the stable solution given by the averaged equation. The double-site solutions have regions of instability that depend on the system's parameters. Figure 4 shows the maximal growth rate of the instability as a function of the dc strength of the nonlinearity and of the coupling constant. We see that the in-phase solutions present instability intervals

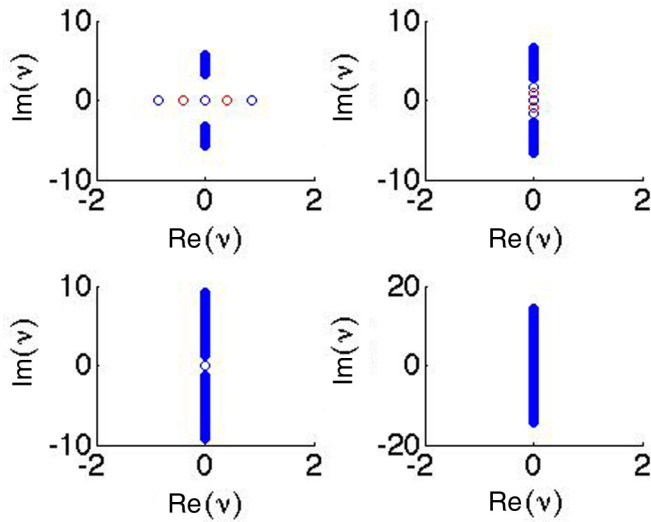


FIG. 5. (Color online) The panels show eigenvalues in the complex plane for selected parameters corresponding to a horizontal cut on the top left panel of Fig. 4 (in-phase solution), obtained by setting $\gamma_0 = 1.75$. For $\kappa = 0$ (not shown) the eigenvalues are purely imaginary and four eigenvalues are zero. For small nonzero κ there are only two zero eigenvalues and the other two previously zero eigenvalues have begun to increase in magnitude on the real axis; this is shown for $\kappa = 0.01$ (red) and $\kappa = 0.3$ (blue) in the top left panel. As κ increases the solution stabilizes and these real eigenvalues move back towards zero horizontally along the real axis. For even higher κ values (at which the solution remains stable), the two eigenvalues increase in magnitude again from zero, but this time along the imaginary axis; this is shown for $\kappa = 0.4$ (red) and $\kappa = 0.5$ (blue) in the top right panel. These eigenvalues merge with the band of eigenvalues on the imaginary axis while the (continuous spectrum) band lengthens; this is shown for $\kappa = 1$ in the bottom left panel. At even higher κ values, two complex conjugate purely imaginary eigenvalues emerge from the band at a magnitude higher than any eigenvalue in the band; this is depicted in the bottom right panel for $\kappa = 5$. The eigenvalues in the bottom right panel that appear to have a very small nonzero real part are seen to actually have a zero real part when the eigenvalues are computed for a much higher lattice length L .

near the uncoupled limit (but contrary to what is the case in the regular DNLS, these instability intervals end at a finite value of the coupling). On the other hand, for the out-of-phase solutions, the instability intervals arise for an intermediate range of the couplings, a feature to which we will return below. Interestingly, we also find that an increase in the index j of the zero of the Bessel function J_0 decreases the size of the region of instability. Additional analysis has shown that for the double-site in-phase solution, an increase in the parameter α (i.e., decrease in frequency $\Omega/2\pi$ of the γ function) decreases the size of the region of instability when plotted versus the coupling κ and the dc nonlinearity strength γ_0 as in Fig. 4. For the double-site out-of-phase solution, an increase in the parameter α (i.e., decrease in frequency $\Omega/2\pi$ of the γ function) expands the region of instability when plotted versus κ, γ_0 as in Fig. 4.

The nature of the double-site instabilities is more clearly demonstrated in Figs. 5 and 6. For the double-site in-phase

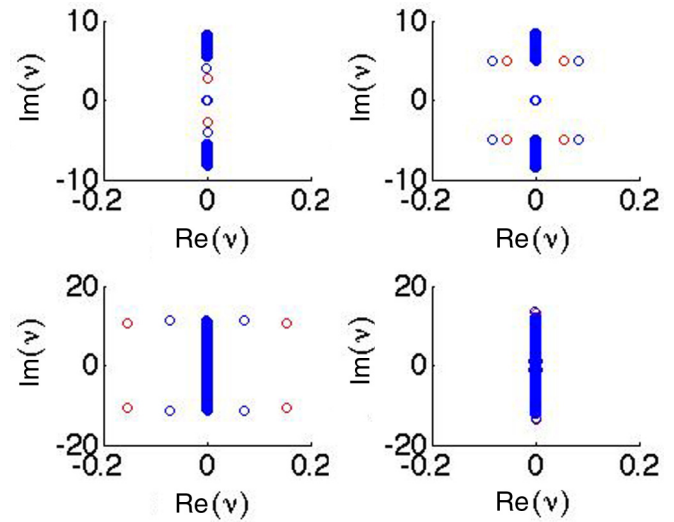


FIG. 6. (Color online) The figure is similar to Fig. 5, but here we select parameter values according to a horizontal cut on the top right panel of Fig. 4 (out-of-phase solution) by setting $\gamma_0 = 3$. For $\kappa = 0$ (not shown) the eigenvalues are purely imaginary and four eigenvalues are zero. For small nonzero κ there are only two zero eigenvalues and the other two previously zero eigenvalues have begun to increase in magnitude on the imaginary axis; this is shown for $\kappa = 0.2$ (red) and $\kappa = 0.35$ (blue) in the top left panel. After the two merge with the (continuous spectrum) band of eigenvalues on the imaginary axis a quartet of complex eigenvalues then emerges for higher κ ; this is depicted for $\kappa = 0.445$ (red) and $\kappa = 0.45$ (blue) in the top right panel. For higher κ values the four complex eigenvalues move in the complex plane, first increasing in real and imaginary parts and then decreasing in the real part until they merge again with the imaginary axis (meanwhile the continuous spectrum band on the imaginary axis lengthens); the bottom two plots show this restabilization with $\kappa = 1.3$ (red) and $\kappa = 1.38$ (blue) in the bottom left panel and $\kappa = 1.7$ in the bottom right panel. At the higher κ values (at which the solution remains stable) two complex conjugate purely imaginary eigenvalues emerge from the band at a magnitude higher than any eigenvalue in the band.

solutions, unstable eigenvalues constitute a pair of equal in magnitude and opposite real numbers; see Fig. 5 where more details of the transition between stability and instability are discussed. A key feature of the double-site in-phase (in)stability is that for fixed γ_0 , small nonzero κ values give unstable solutions and higher κ values stabilize the solution, a feature that is typically *absent* in the standard DNLS model. For the double-site out-of-phase solutions, unstable eigenvalues appear as a quartet (due to the Hamiltonian nature of the system), i.e., two complex conjugate pairs with equal magnitude plus or minus real parts. This arises from the collision of the two imaginary eigenvalues (in this case), stemming from the origin with the continuous spectrum, a feature that is common in such out-of-phase focusing nonlinearity settings (see, e.g., [28]). More details of the transitions between stable and unstable solutions for the out-of-phase solutions are discussed in Fig. 6. A key feature of the double-site out-of-phase (in)stability is that for fixed γ_0 , both small nonzero and large positive κ values give stable solutions with the unstable region lying in a finite κ interval that lies away from $\kappa = 0$. For large κ , the formerly

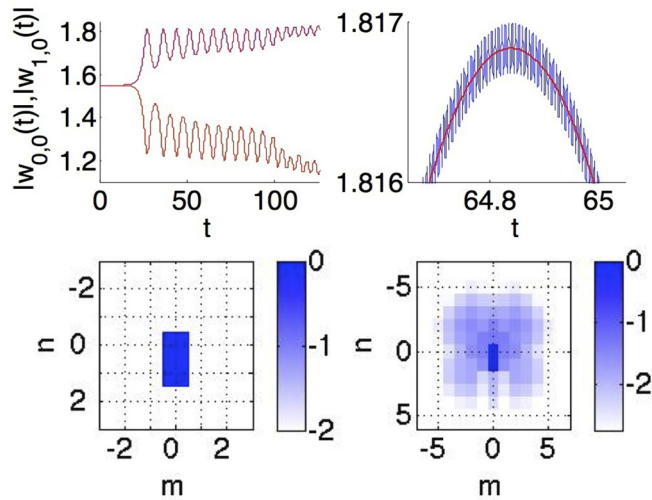


FIG. 7. (Color online) The plots show the result of propagation of the double-site in-phase exact compacton solution in the time parameter t according to each of the equations (1) and (5). The values of ϵ , Ω , γ_1 , and α are the same as in Fig. 4. In the bottom left panel the plot shows $\log_{10}(|u_{n,m}(0)|)$ plotted as a function of n, m , where $u_{n,m}(0) = v_{n,m}(0)$ is the initial double-site in-phase compacton configuration at $t = 0$; this plot, of course, shows an order 0 logarithmic amplitude at the two excited sites and vanishing amplitude elsewhere. The instability strength for this solution is $\max[\text{real}(\nu)] \approx 0.5327$. In the bottom right panel the plot shows $\log_{10}[|v_{n,m}(80)|]$, where $v_{n,m}(t)$ is determined from $v_{n,m}(0)$ according to the averaged equation (5); the plot of $\log_{10}[|u_{n,m}(80)|]$ determined from the nonautonomous equation (1) is visually indistinguishable from the averaged version shown in the bottom right panel. In the bottom right panel plot we see small-amplitude excitations appearing near the compacton site and these small amplitudes continue to spread out spatially as t increases, while the central sites have amplitudes that approach nonzero values. The top left panel shows this evolution of the amplitude of the two excited sites over time with the unaveraged magnitudes $|w_{0,0}(t)| = |u_{0,0}(t)|$ in blue and $|w_{1,0}(t)| = |u_{1,0}(t)|$ in green; these are propagated according to (1). The overlying red line plots correspond to the magnitudes $|w_{0,0}(t)| = |v_{0,0}(t)|$ and $|w_{1,0}(t)| = |v_{1,0}(t)|$ propagated according to the averaged equation (5). From the perspective displayed in the top left panel the averaged and the unaveraged amplitudes seem to lie on top of one another. The top right panel here shows a small portion of the same plot zoomed in so as to show how the averaged solution in red in fact averages the nonautonomous equation solution (over a period of the nonlinearity prefactor variation) in blue.

unstable quartet grows (in the imaginary part) faster than the band of the continuous spectrum and eventually returns to the imaginary axis, leading to spectral stability.

For stable solutions in the averaged model the amplitudes of the excited sites remain steady at the predicted value A_0 in Eq. (9) or oscillate around it, if perturbed; this is the same feature described above for stable single-site and vortex-type solutions. For stable solutions in the original nonautonomous model the amplitudes oscillate about the value A_0 as expected.

In Fig. 4 the green dots show select parameter values for which the dynamics of unstable double-site solutions will be explored below. Recall that in the case of the double-site solutions, Eq. (9) gives the amplitudes of the two excited

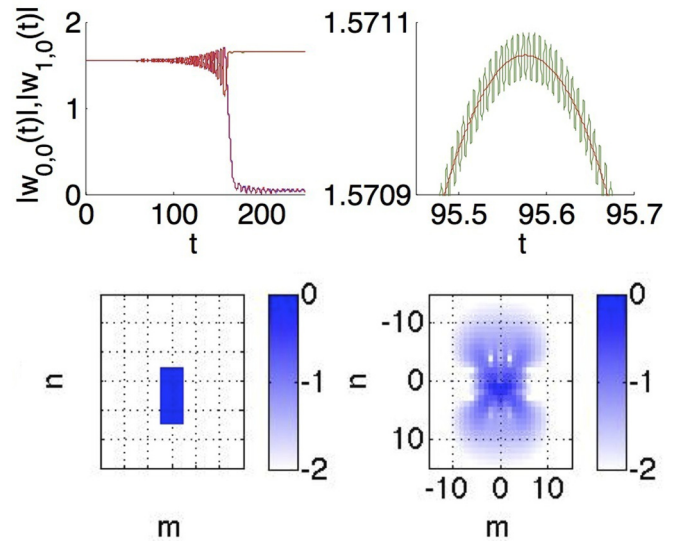


FIG. 8. (Color online) The plots are similar to Fig. 7, with the same parameter values, but here for the double-site out-of-phase compacton solution; also the bottom right panel here corresponds to $t = 180$. The instability strength for this solution is $\max[\text{real}(\nu)] \approx 0.0298$. Notice that here the eventual evolution leads to a single-site excitation (see the amplitude evolution in the top left panel and the eventual profile in the bottom right panel).

sites $u_{0,0}, u_{1,0}$ at $t = 0$. In Figs. 7 and 8 plots of the evolution of the amplitudes of the unstable double-site solutions over the propagation parameter t are shown in detail, according to the averaged equation (5) and the original nonautonomous equation (1). The unstable double-site solutions (both in-phase and out-of-phase) transition to a noncompacton state with oscillating phase so that the initial phase profile is not preserved over time. For the double-site in-phase solution in Fig. 7 the two initially excited sites remain of order one amplitude as t increases (although the solution mass is asymmetrically distributed between them due to their different amplitudes after the instability manifestation). For sites in the vicinity of the original compact support, there is gain in small amplitudes increasing the footprint of the solution. For the double-site out-of-phase solution in Fig. 8, as t increases the amplitude at the two center sites first oscillates and then one of the sites' amplitudes drops down towards zero; the resulting configuration is a noncompacton solution with order one magnitude only at one site, i.e., the waveform degenerates towards a fundamental, single-site solution.

In Fig. 9 we show plots of the dependence of the instability strength (i.e., of the maximal growth rate of the potential unstable modes) on the parameter grid for the four- and five-site solutions. The stability properties of both the four-site symmetric (in-phase) compacton and the five-site compacton configurations follow a pattern similar to that of the double-site in-phase solutions; compare the leftmost and rightmost plots of Fig. 9 to the left column of Fig. 4. That is, for fixed γ_0 , as κ increases from zero the solutions are immediately unstable with real eigenvalues and then they eventually stabilize for higher values of the coupling κ . The eigenvalues for the unstable solutions appear in real pairs similar to that shown in Fig. 5. While the double-site in-phase solutions have only

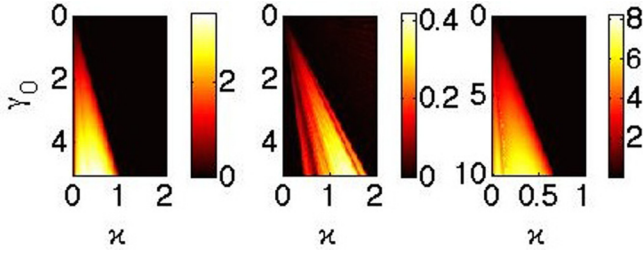


FIG. 9. (Color online) This figure is similar to Fig. 4, but here the parameter values common across all four plots are $L = 11$, $\epsilon = 0.01$, and $\Omega = \gamma_1 = 10$ so that $\alpha = 1$. The leftmost plot is associated with a four-site symmetric solution using the first zero of the Bessel function with $j = 1$, the middle plot corresponds to a four-site antisymmetric solution with $j = 1$, and the rightmost plot is for the five-site solution with $j = 5$. The axis labels are the same as those established in Fig. 4.

one pair of real nonzero eigenvalues, the four-site symmetric solutions have three pairs of real nonzero eigenvalues and the five-site unstable solutions have four pairs. This is in line with the expectations from the standard DNLS model [28].

The stability properties of the four-site antisymmetric solutions (with adjacent sites being out of phase) follow a pattern similar to that of the double-site out-of-phase solutions, where for small enough κ the solutions are stable. Increasing κ , one finds a finite (intermediate coupling) interval of instability and then for higher κ the solution stabilizes again. To see the similarity between the four-site antisymmetric solution stability and the double-site out-of-phase stability compare the center plot of Fig. 9 to the right column of Fig. 4. Plots of the eigenvalues in the complex plane look similar to the plots in Fig. 6. While the double-site out-of-phase solutions feature for small coupling a single imaginary eigenvalue pair and thus have only one potential quartet of unstable eigenvalues, the four-site antisymmetric solutions have three imaginary pairs for small κ and may eventually feature up to three eigenvalue quartets, again in line with what one may expect in the standard DNLS case [28].

V. CONCLUSION AND FUTURE CHALLENGES

Summarizing the findings of the present work, we have illustrated through a combination of analytical considerations and numerical results the existence of 2D compactons of the discrete nonlinear Schrödinger equation in the presence of fast periodic time modulations of the nonlinearity. In particular, we showed that single-site multidimensional compactons are very robust excitations; two-site stationary compactons, of both symmetric and antisymmetric type, are also quite generic and can be stable in a wide region of the parameter space (of the coupling and nonlinearity prefactors). Four-site compactons have been found to be always stable only in the vortex state, an unusual feature that is fundamentally distinct from the case of the standard discrete nonlinear Schrödinger model. The five-site compactons may also feature instabilities but can be again controllably stabilized for suitable parametric intervals of the tunneling constant and/or dc nonlinearity strength. These findings not only were obtained for the effective averaged DNLS equation that was derived herein, but were

also confirmed by means of direct numerical simulations of the original nonautonomous DNLS model.

It is relevant to point out that excitations of the form considered herein should in principle be accessible to state-of-the-art current experiments in the optical (waveguide array) or atomic (Bose-Einstein condensate) realm. For instance, in the BEC context, such states could be obtained by considering a 2D array of ^{85}Rb or ^7Li created with a deep two-dimensional optical lattice. In this case, the corresponding prototypical mean-field model for the bosonic wave function ψ would read

$$i\hbar\psi_t = -\frac{\hbar^2}{2m}\nabla^2\psi + g_{2D}|\psi|^2\psi + V_0[\sin^2(kx) + \sin^2(ky)]\psi, \quad (19)$$

where g_{2D} is the effective nonlinear prefactor (see, e.g., [34]), V_0 characterizes the strength, and k is the period of the optical lattice. In the (superfluid) limit of a deep optical lattice, e.g., $V_0 \gg E_R = \hbar^2 k^2 / 2m$, this equation reduces to the DNLS model [29]. For ^7Li one could use the Feshbach resonance technique at the external magnetic field of $B_0 = 738$ G with the width $\Delta B = -170$ G [35] to modulate the interactions. The background scattering length can be taken as $a_{\text{bg}} \approx -20a_B$, where a_B denotes the Bohr radius. The time dependence of the scattering length $a_s(t) = a_{s0} + a_{s1} \cos(\omega t)$ follows from the variation of the magnetic field in time according to

$$a_s(B) = a_{\text{bg}} \left(1 - \frac{\Delta}{B - B_0} \right).$$

For $B(t) = [970 \pm 155 \cos(\omega t)]$ G, we have $a_{s0} = -5a_B$ and $a_{s1} = 10a_B$. Using suitable lattice parameters such as $2\pi/k = 0.5 \mu\text{m}$ and $V_0 = 15E_R$, we can ensure being in the regime of applicability of the DNLS model, enabling, under the above conditions, the experimental realizability of the higher-dimensional discrete compactons.

On the other hand, there are numerous interesting themes for future theoretical investigations. It would be interesting to examine in more detail the origin of features that are fundamentally different between the averaged model considered herein and the standard DNLS model. These include the restabilization of in-phase configurations and the absence of instabilities for the discrete vortex configuration. Additionally, it would be especially interesting to explore the approach of the model to the continuum limit of large coupling. It is well known that collapse features emerge as the DNLS model approaches the continuum limit [28], although this may happen in unconventional ways for nonstandard discretizations of the model (see, e.g., [36]). It would be intriguing to explore the properties of the present discretization (and of the original nonautonomous model) as this limit is approached. Finally, it would also be of interest and relevance to explore three-dimensional configurations in analogy to ones of the standard DNLS model [28] and to examine their stability properties. Such studies are currently in progress and will be reported in the future.

ACKNOWLEDGMENTS

M.S. acknowledges partial support from the Ministero dell'Istruzione, dell'Università e della Ricerca through a Programmi di Ricerca Scientifica di Rilevante Interesse

Nazionale initiative under Grant No. 2010HXAW77-005. P.G.K. gratefully acknowledges the support from NSF-DMS-1312856, BSF-2010239, the US AFOSR under Grant No. FA9550-12-1-0332, and the ERC under FP7, Marie Curie Actions, People, International Research Staff Exchange Scheme

(IRSES-605096). The work of P.G.K. at Los Alamos was partially supported by the US Department of Energy. F.K.A. acknowledges support from a senior visitor fellowship from CNPq (Brazil).

-
- [1] B. A. Malomed, *Soliton Management in Periodic Systems* (Springer, Berlin, 2006).
- [2] H. Lignier, C. Sias, D. Ciampini, Y. Singh, A. Zenesini, O. Morsch, and E. Arimondo, *Phys. Rev. Lett.* **99**, 220403 (2007).
- [3] A. Szameit, Y. V. Kartashov, F. Dreisow, M. Heinrich, T. Pertsch, S. Nolte, A. Tünnermann, V. A. Vysloukh, F. Lederer, and L. Torner, *Phys. Rev. Lett.* **102**, 153901 (2009).
- [4] F. K. Abdullaev, P. G. Kevrekidis, and M. Salerno, *Phys. Rev. Lett.* **105**, 113901 (2010).
- [5] F. K. Abdullaev, M. S. A. Hadi, M. Salerno, and B. A. Umarov, *Phys. Rev. A* **90**, 063637 (2014).
- [6] P. Rosenau and J. M. Hyman, *Phys. Rev. Lett.* **70**, 564 (1993).
- [7] P. Rosenau, *Phys. Rev. Lett.* **73**, 1737 (1994).
- [8] P. Rosenau, J. M. Hyman, and M. Staley, *Phys. Rev. Lett.* **98**, 024101 (2007).
- [9] V. V. Konotop and S. Takeno, *Phys. Rev. E* **60**, 1001 (1999).
- [10] P. G. Kevrekidis and V. V. Konotop, *Phys. Rev. E* **65**, 066614 (2002); P. G. Kevrekidis, V. V. Konotop, and S. Takeno, *Phys. Lett. A* **299**, 166 (2002); P. G. Kevrekidis, V. V. Konotop, A. R. Bishop, and S. Takeno, *J. Phys. A* **35**, L641 (2002).
- [11] B. Dey, M. Eleftheriou, S. Flach, and G. P. Tsironis, *Phys. Rev. E* **65**, 017601 (2001).
- [12] P. Jason and M. Johansson, *Phys. Rev. A* **85**, 011603 (2012); **88**, 033605 (2013).
- [13] Y. V. Kartashov, V. V. Konotop, and L. Torner, *Phys. Rev. B* **86**, 205313 (2012).
- [14] J. M. English and R. L. Pego, *Proc. Am. Math. Soc.* **133**, 1763 (2005); A. Stefanov and P. Kevrekidis, *J. Nonlinear Sci.* **22**, 327 (2012).
- [15] R. A. Vicencio and M. Johansson, *Phys. Rev. A* **87**, 061803(R) (2013); M. Johansson, U. Naether, and R. A. Vicencio, *Phys. Rev. E* **92**, 032912 (2015).
- [16] R. A. Vicencio, C. Cantillano, L. Morales-Inostroza, B. Real, C. Mejía-Cortés, S. Weimann, A. Szameit, and M. I. Molina, *Phys. Rev. Lett.* **114**, 245503 (2015).
- [17] A. Rapp, X. Deng, and L. Santos, *Phys. Rev. Lett.* **109**, 203005 (2012).
- [18] S. Greschner, L. Santos, and D. Poletti, *Phys. Rev. Lett.* **113**, 183002 (2014).
- [19] S. Greschner, G. Sun, D. Poletti, and L. Santos, *Phys. Rev. Lett.* **113**, 215303 (2014).
- [20] D. Bazeia, L. Losano, M. A. Marques, and R. Menezes, *Phys. Lett. B* **736**, 515 (2014).
- [21] P. Rosenau and E. Kashdan, *Phys. Rev. Lett.* **101**, 264101 (2008).
- [22] P. Rosenau and E. Kashdan, *Phys. Rev. Lett.* **104**, 034101 (2010).
- [23] H. Saito and M. Ueda, *Phys. Rev. Lett.* **90**, 040403 (2003).
- [24] F. K. Abdullaev, J. G. Caputo, R. A. Kraenkel, and B. A. Malomed, *Phys. Rev. A* **67**, 013605 (2003).
- [25] B. B. Baizakov, V. V. Konotop, and M. Salerno, *J. Phys. B* **35**, 5105 (2002).
- [26] B. B. Baizakov, B. A. Malomed, and M. Salerno, *Europhys. Lett.* **63**, 642 (2003).
- [27] M. Oster and M. Johansson, *Physica D* **238**, 88 (2009).
- [28] P. G. Kevrekidis, *The Discrete Nonlinear Schrödinger Equation* (Springer, Heidelberg, 2009).
- [29] A. Trombettoni and A. Smerzi, *Phys. Rev. Lett.* **86**, 2353 (2001); F. K. Abdullaev, B. B. Baizakov, S. A. Darmanyan, V. V. Konotop, and M. Salerno, *Phys. Rev. A* **64**, 043606 (2001); G. L. Alfimov, P. G. Kevrekidis, V. V. Konotop, and M. Salerno, *Phys. Rev. E* **66**, 046608 (2002).
- [30] G. Assanto, L. A. Cisneros, A. A. Minzoni, B. D. Skuse, N. F. Smyth, and A. L. Worthy, *Phys. Rev. Lett.* **104**, 053903 (2010).
- [31] M. Centurion, M. A. Porter, P. G. Kevrekidis, and D. Psaltis, *Phys. Rev. Lett.* **97**, 033903 (2006); M. Centurion, M. A. Porter, Y. Pu, P. G. Kevrekidis, D. J. Frantzeskakis, and D. Psaltis, *ibid.* **97**, 234101 (2006).
- [32] D. E. Pelinovsky, P. G. Kevrekidis, D. J. Frantzeskakis, and V. Zharnitsky, *Phys. Rev. E* **70**, 047604 (2004).
- [33] A. Eckardt, C. Weiss, and M. Holthaus, *Phys. Rev. Lett.* **95**, 260404 (2005).
- [34] P. G. Kevrekidis, D. J. Frantzeskakis, and R. Carretero-González, *Emergent Nonlinear Phenomena in Bose-Einstein Condensates* (Springer, Berlin, 2008).
- [35] P. Dyke, S. E. Pollack, and R. G. Hulet, *Phys. Rev. A* **88**, 023625 (2013).
- [36] P. G. Kevrekidis, G. J. Herring, S. Lafortune, and Q. E. Hoq, *Phys. Lett. A* **376**, 982 (2012).